Progress in Nb_3Sn RRP Strand Studies and Rutherford Cable Development at FNAL

E. Barzi, D. Turrioni, and A.V. Zlobin

***Abstract*—A strong push to Nb_3Sn conductor development in the U.S. as well as in Europe has been driven by the development of Nb_3Sn dipoles and quadrupoles for the LHC luminosity upgrades. Rutherford cables with high aspect ratio are used for these magnets to achieve large fields and gradients at relatively low currents. At Fermilab 40-strand keystoned cables with and without a stainless steel core were developed and produced using 0.7 mm Nb_3Sn strands made by Oxford Superconducting Technology (OST) with 127 and 169 restacks using the Restacked-Rod-Process® (RRP®) with either NbTa alloy or Ti doping. The performance and properties of such strands and cables are compared to evaluate possible candidates for the production magnets of the LHC upgrades. The electrical performance was first compared for wires under flat-rolling deformation, and then in cables made with different processes and geometries. The round wires are also compared under tensile and compressive strain using a Walters' spring variable-temperature probe that was recently commissioned at FNAL. Finally cable test results obtained with a 14 T/ 16 T Rutherford cable test facility with bifilar sample and superconducting transformer are shown.**

***Index Terms*—Accelerator magnet, Nb_3Sn wires, Rutherford cable, subelement.**

I. Introduction

To achieve magnetic fields of ~10-15 T in superconducting accelerator magnets, A15 superconducting strands (Nb_3Sn or Nb_3Al) with high critical current density J_c and stable quench performance are being developed [1], [2]. All high field magnets are subject to large Lorentz forces and large stored energies, which impose large strains on the conductor. Because the J_c of A15 superconducting wires is highly sensitive to strain, the latter represents one of the main limitations in the design and operation of high field magnets. In addition, accelerator magnets have stringent field quality requirements. The superconducting subelement size has to be below certain limits to provide conductor stability to "flux jumps" and an acceptable persistent current effect. To mitigate inductance, the winding is composed of so-called Rutherford-type cables, which pack together dozens of single round strands. In a Rutherford cable the round wires see large and complicated deformations, which bring them into the plastic regime. This typically modifies the inner architecture of the wires, which in turn impacts their electrical and magnetic properties. For all of these reasons, a sound conductor qualification plan is important to evaluate and select strands that are adequate for magnet operation in a real machine.

The conductor qualification plan developed at FNAL to evaluate and select adequate strands for accelerator magnet operation should include the following steps:

- Procurement of billets from industry in sufficiently large quantities to aim at production quality.
- Qualification of round and deformed strands for J_c, *RRR*, stability and J_c strain sensitivity.
- Rutherford cable development and fabrication.
- Characterization of strands extracted from cables.
- Cable test.

Such conductor qualification plan is the first step towards the final and ultimate test of the conductor in a magnet model.

The FNAL accelerator magnet R&D program (High Field Magnet program) is executing and expending this plan in order to develop and demonstrate Nb_3Sn strands based on the RRP® process and Rutherford cables for high-field accelerator magnets. In this paper, an example of the above conductor qualification plan is used for the latest 169-stack RRP® wire developed by OST. When applicable, the results are compared with those from previous RRP® wire designs and results of their tests in magnet models. Recommendations for Nb_3Sn strand design parameters for production quadrupoles [3] and dipoles [4] for the LHC luminosity upgrades and for R&D magnets for the Muon Storage Ring and Interaction Region of a Higgs Factory [5] are formulated.

II. Strand and Cable Sample Parameters

A. Strand Description

Table I shows parameters of the 108/127 RRP® (RRP1), the 150/169 RRP® (RRP2) and the 132/169 RRP® (RRP3 and RRP4) strands produced by OST and used in these studies. Pictures of the cross-sections are shown in Fig. 1. In Table I, D_S is the geometrical subelement size of the flat to flat dimension of the hexagonal outer diffusion barrier, as calculated from design, unreacted. The heat treatments shown in Table I are the nominal ones for use in magnets. They were also used for the wires in this study unless otherwise specified.

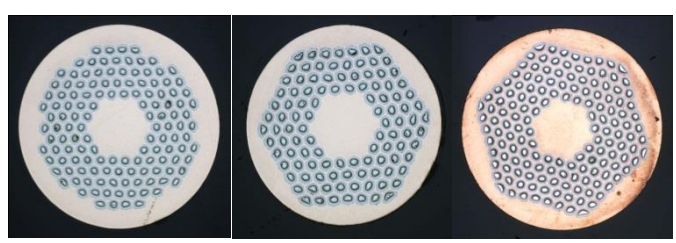

Fig. 1. Cross sections of 108/127 RRP® (left), 132/169 RRP® (center), 150/169 RRP® (right) strands.

Manuscript received July 17, 2013. This work was supported in part by Fermi Research Alliance, LLC, under Contract DE-AC02-07CH11359 with the US Department of Energy.

All authors are with Fermilab National Accelerator Laboratory, Batavia, IL 60510, USA (e-mail: barzi@fnal.gov).

TABLE I
STRAND PARAMETERS

Strand ID	RRP1	RRP2	RRP3	RRP4
Stack design	108/127	150/169	132/169	132/169
Ternary element	Ta	Ta	Ti	Ti
Production year	2010	2011	2009	2012
Diameter d, mm	0.7	0.7	0.7	0.7
I_c (4.2K, 12 T), A	421	465	348	449
J_c (4.2K, 12 T), A/mm^2	2,460	2,508	2,138	2,649
I_c (4.2K, 15 T), A	201	230	163	219
J_c (4.2K, 15 T), A/mm^2	1176	1240	1001	1297
D_S, μm	41	36	36	36
Twist pitch, mm	14	14	17	13
Cu fraction λ, %	55.5	51.8	57.7	56.0
RRR	83-359	165	76	153
Final HT step	640ºC/48h	665ºC/50h	640ºC/48h	640ºC/48h

B. Cable Development and Fabrication

A cored cable technology to suppress eddy currents and obtain better field quality and ramp rate dependence in magnets had been developed using a two-step fabrication approach, with and without intermediate anneal, and tested [6]. After the commissioning of a new turk-head designed for one-pass cable fabrication (Fig. 2), similar cable geometries were reproduced in one pass (therefore without an intermediate annealing step) using 132/169 RRP® (RRP3 and RRP4) strands. Table II summarizes the parameters of these keystoned cables. The cross section of one of these cables is shown in Fig. 3. All cables had a 25 μm thick stainless steel core. The core in cables 1 to 6 was 11.0 mm wide, that used in cables 7 to 9 was 11.7 mm wide, and that used in cables 10 to 12 in one pass was 9.5 mm wide. Cables 1 to 9 are from [6].

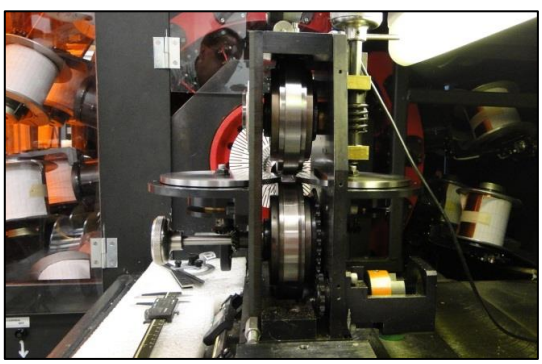

Fig. 2. Turk-head for one-pass cable fabrication [6].

TABLE II
CABLES FOR DEVELOPMENT OF CORED* CABLE TECHNOLOGY

Cable ID	Step (No.)	RRP® wire design	Width before/after keystoning (mm)	Mid-thickness before/after keystoning (mm)	*PF* before/after keystoning (%)	Annealing step
1	2	RRP2	14.48/14.66	1.320/1.270	84.8/87.1	No
2	“	“	14.48/14.66	1.320/1.253	84.8/88.3	“
3	“	“	14.48/14.68	1.320/1.230	84.8/89.8	“
4	2	RRP2	14.57/14.68	1.338/1.270	83.4/86.8	Yes
5	“	“	14.57/14.68	1.338/1.251	83.4/88.4	“
6	“	“	14.57/14.69	1.338/1.232	83.4/89.6	“
7	2	RRP1	14.59/14.70	1.336/1.270	83.0/86.7	Yes
8	“	“	14.59/14.70	1.336/1.252	83.0/87.9	“
9	“	“	14.59/14.71	1.336/1.230	83.0/89.4	“
10	1	RRP3, RRP4	-/ 14.75	-/ 1.271	-/ 85.7	No
11	“	“	-/ 14.71	-/ 1.250	-/ 87.4	“
12	“	“	-/ 14.73	-/ 1.230	-/ 88.8	“

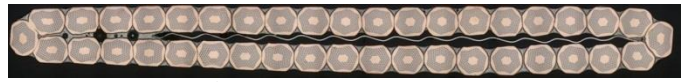

Fig. 3. Cross section of keystoned cable made with 150/169 RRP® strands and a stainless steel core 11 mm wide and 25 μm thick [6].

III. SAMPLE PREPARATION AND MEASUREMENT PROCEDURE

For standard I_c measurements of round, deformed and extracted strands, the samples were wound on grooved cylindrical barrels made of Ti-alloy, and heat treated in Argon. After reaction, the samples were tested on the same barrel. Splices soldered in parallel to sample end turns were used in the transition area from the Cu to the Ti-alloy section of the barrel. STYCAST was used to bond the sample. In standard I_c measurements, 3 pairs of voltage taps were used. Two pairs were placed at the center of the sample 50 cm and 75 cm apart, and one pair at the Cu leads to be used for quench protection. The I_c was determined from the voltage-current (V-I) curve using the 10^{-14} Ω·m resistivity criterion. Typical I_c measurement uncertainties are within ±1% at 4.2 K and 12 T.

The critical current density in the non-Cu part of the strand cross-section, J_c, was defined as $I_c/S/(1-\lambda)$ where S is the strand cross-section and λ is the Cu fraction.

Deformation was applied by a motorized roller system to round wires before any reaction to flatten the strand vertically, and the wire is free to expand laterally. Wire deformation was defined as $(d_0-t)/d_0$, where d_0 is the original strand diameter and t the thickness of the deformed strand.

The RRR was measured using a devoted probe.

J_c strand sensitivity to longitudinal strain was measured using a Walters’ spring-type device [7] as described in Appendix.

Cable I_c measurements were performed with an upgraded Rutherford cable test facility [8] with bifilar sample and superconducting transformer that operates in a 14 T/16 T Teslatron system by Oxford Instruments.

IV. EXPERIMENTAL RESULTS AND DISCUSSION

A. Qualification of Round and Deformed Strands

RRP4 wires of the 132/169 RRP® design were flat-rolled to increasing deformations to systematically study such dependence of their properties. Figures 4 and 5 compare the J_c and V-I test results at 4.2 K as function of magnetic field between the 0.7 mm round and rolled 132/169 RRP® (RRP4) and the 1 mm round and rolled 108/127 RRP® (RRP1) [9] strands. The former wire has a slightly larger J_c(12 T) and is representative of a ~40 μm subelement size D_S, and the latter has a D_S of ~60 μm. Close markers were used when an accurate I_c was obtained from the V-I curve, whereas open markers indicate the maximum current reached by samples that quenched prematurely. At 40% deformation, where an homogeneous comparison can be made, for the wire with a D_S that is 50% larger, the minimum stable current density obtained in the V-I measurements as a function of field (Fig. 5) is half that of the wire with a D_S of 40 μm (Fig. 4).

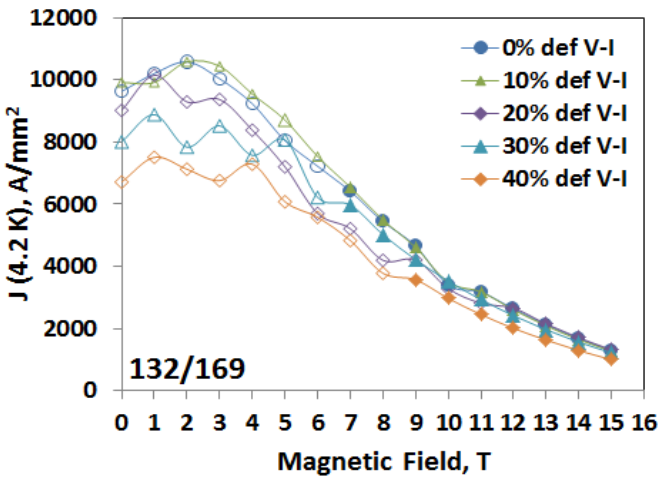

Fig. 4. J_c and *V-I* test results at 4.2 K as function of magnetic field for the 0.7 mm round (~40 µm subelement size) and rolled 132/169 RRP® (RRP4) strands. Closed markers indicate I_c values, and open markers show premature quenches.

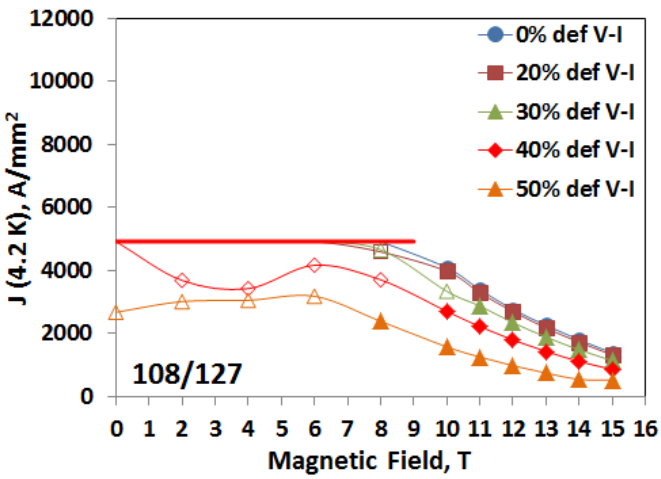

Fig. 5. J_c and *V-I* test results at 4.2 K as function of magnetic field for the 1 mm round (~60 µm subelement size) and rolled 108/127 RRP® (RRP1) strands [9]. Closed markers indicate I_c values, and open markers show premature quenches. Horizontal line indicates power supply limit.

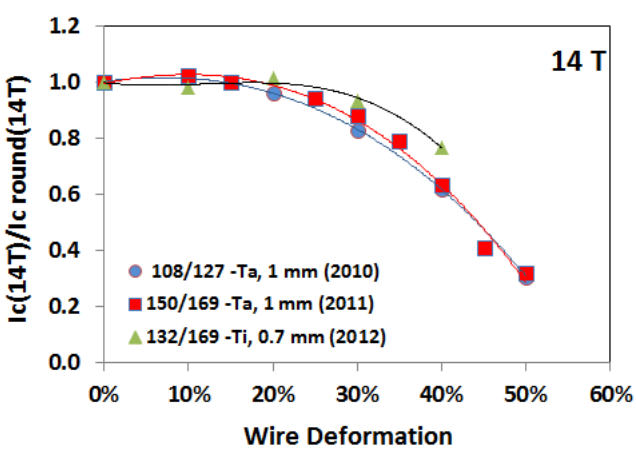

Fig. 6. I_c (14 T) of the rolled strand normalized to that of a round strand as function of wire deformation for wires RRP1, RRP2 [9] and RRP4.

Fig. 6 compares the I_c (14 T) of the rolled strand normalized to that of a round strand as function of wire deformation for wires RRP1, RRP2 [9] and RRP4. Whereas the I_c of the RRP1 and RRP2 wires, which both have Ta as ternary element, degrade similarly under increasing flat-rolling deformation, the RRP 4 wire with Ti doping retains larger values of critical current (~80% of I_c at 40% deformation) at the same deformation levels.

Fig. 7 compares the RRR of the rolled strand as function of wire deformation for wires RRP1, RRP2 [9] and RRP4. For this specific billet of RRP4 wire design, at 40% deformation the *RRR* is larger than 50. However, there can be substantial variability in *RRR* between billets of same design during the design development and optimization process in industry. An example is given in Fig. 8, which shows the *RRR* of the rolled strand as function of wire deformation for different billets of the 108/127 RRP® (RRP1) design that were heat treated with same heat treatment cycle.

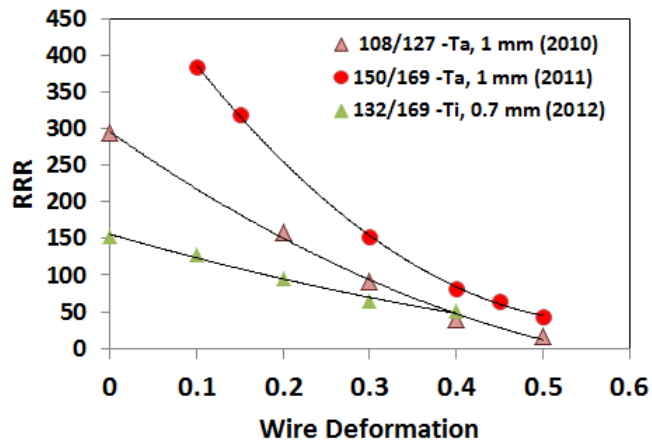

Fig. 7. *RRR* of the rolled strand as function of wire deformation for wires RRP1, RRP2 [9] and RRP4.

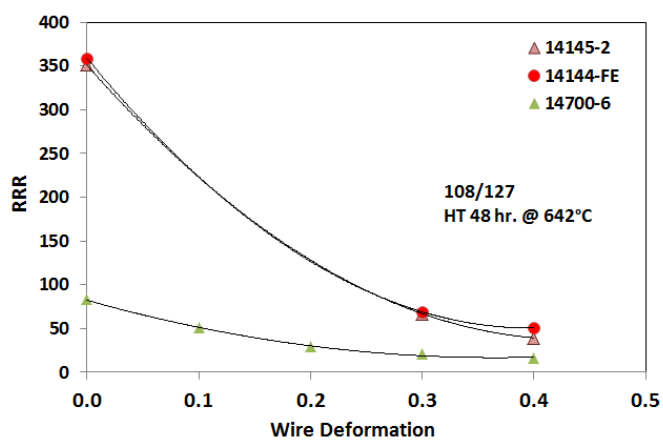

Fig. 8. *RRR* of the rolled strand as function of wire deformation for different billets of the 108/127 RRP® (RRP1) design.

B. Characterization of Strands Extracted from Cables

Figs. 9 and 10 compare the I_c(12 T) and the *RRR* of the extracted strand as function of cable mid-thickness for RRP1, RRP2 [6], RRP3 and RRP4 wires extracted from cable ID's 1 to 12 from Table II. The "Ann." notation in the legend indicates cables that had undergone an intermediate annealing

process between their first forming stage and their keystoning step (see also Table II). The cables made using 132/169 RRP® (RRP3 and RRP4) strands with Ti doping were made in one pass, therefore without any annealing step. The I_c values of the virgin wires are shown in Table I. One can see from Fig. 9 that the Ti doped wire RRP4 preserved its current carrying capabilities up to large cable compaction factors, even without any annealing. Its maximum I_c degradation at 12 T was ~2% at ~89% cable compaction. This effect of Ti doping possibly strengthening the wire is apparent also from Fig. 10, which shows that the only two wires whose RRR values are independent of cable compaction are the Ti-doped RRP3 and RRP4.

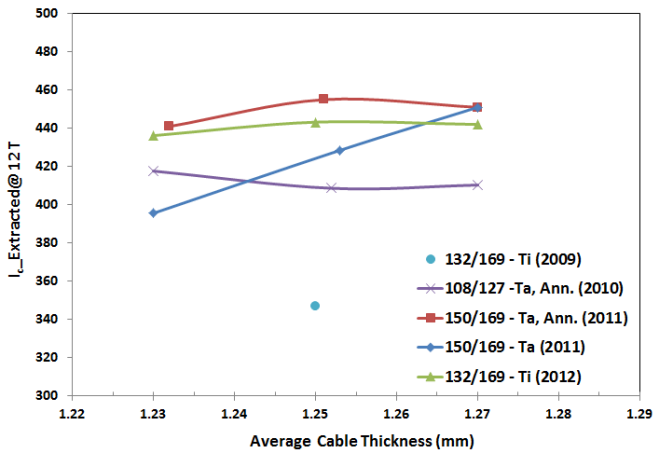

Fig. 9. I_c (12 T) of the extracted strand as function of cable mid-thickness for RRP1, RRP2 [6], RRP3 and RRP4 wires extracted from cable ID's 1 to 12.

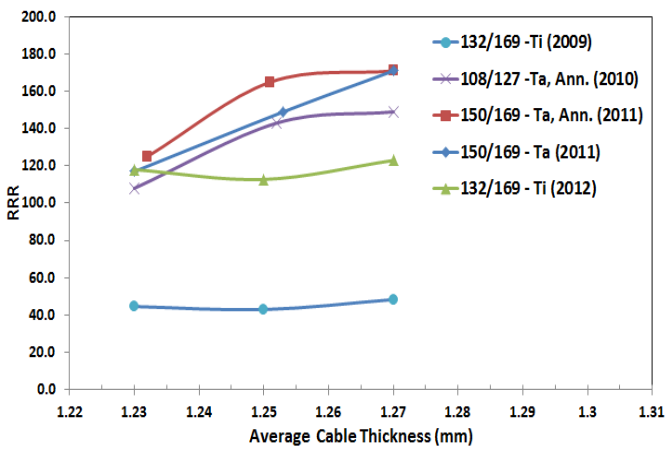

Fig. 10. *RRR* of the extracted strand as function of cable mid-thickness for RRP1, RRP2 [6], RRP3 and RRP4 wires extracted from cable ID's 1 to 12.

C. *Strain Sensitivity Measurements*

The normalized strain behavior of the three 0.7 mm wires described in Table I is compared in Fig. 11, which shows the normalized I_c(4.2 K, 15 T) as function of longitudinal intrinsic strain over channel CH1 for samples of Ta-alloyed 108/127 RRP® (RRP1), Ta-alloyed 150/169 RRP® (RRP2) and Ti-doped 132/169 RRP® (RRP4). The RRP1 and RRP2 strands were given a heat treatment with dwells at 210°C for 48 h, at 400°C for 48 h and at 665°C for 50 h, and the RRP4 strand was given a heat treatment with dwells at 210°C for 48 h, at 400°C for 48 h and at 650°C for 50 h. In all cases, temperature ramp rates to reach the respective dwells were of 25°C/h, 50°C/h and 75°C/h. As shown in Fig. 11, attempts at measuring the irreversible strain were made for Ta-alloyed wire RRP1 as described in Appendix for wire RRP4. As point A in Fig. 11 shows, the RRP1 sample was tested up to +0.11% of intrinsic strain before going back to point A' at lower intrinsic strain, where an I_c value was obtained that was lower than the previous measurement by an amount larger than the I_c measurement precision of 0.1 A. This placed the intrinsic strain of Ta-alloyed RRP1 wire at less than +0.11%, to be compared with the irreversible intrinsic strain range of +0.26% to +0.31% found for the Ti-doped wire RRP4. This is consistent with previous studies by Najib Cheggour et al.

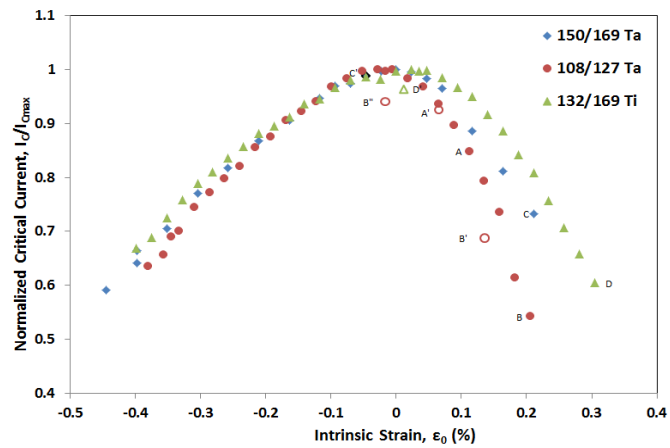

Fig. 11. Normalized I_c(4.2 K, 15 T) as function of longitudinal intrinsic strain over channel CH1 for 0.7 mm samples of Ta-alloyed 108/127 RRP® (RRP1), Ta-alloyed 150/169 RRP® (RRP2) and Ti-doped 132/169 RRP® (RRP4).

D. *Cable Test*

An example of cable quench current results [6] as a function of field is shown in Fig. 12 for the cable that was used in the first 11 T demonstrator dipole developed and tested at FNAL [10]. The keystoned cable was made of RRP1 strands and did not have a SS core [11]. The last step of the cable heat treatment was 50 h at 665°C and it was heat treated together with witness samples of its extracted strands.

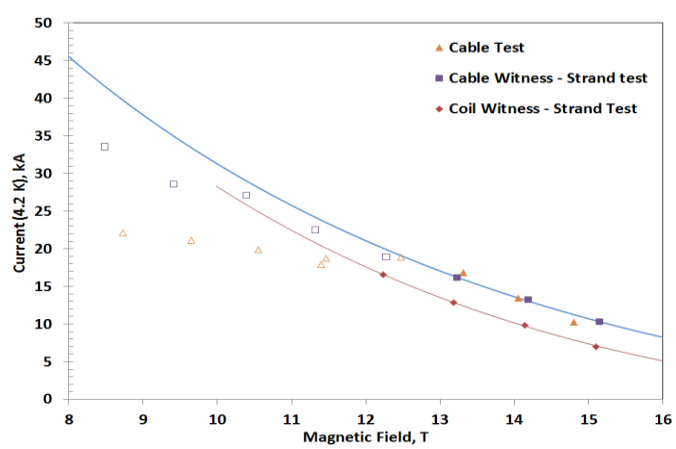

Fig. 12. Cable quench current obtained as function of magnetic field for an insulated Nb_3Sn cable sample made of 40 RRP1 strands and without SS core, which was tested without any epoxy impregnation [6]. Self-field corrections were applied in this plot to both cable and strand test results.

In Fig. 12 the cable test results are compared with its own witness strand samples and also with the witness strand samples that had been used for the dipole coils, whose last step of the heat treatment was 48 h at 640°C, and therefore produced I_c values about 20% smaller, as expected. Closed markers indicate the presence of a *V-I* transition curve during the test, whereas open markers denote abrupt quenches without any smooth voltage transition. Self-field corrections were applied in this plot to both cable and strand test results. The correlation between strand and cable test results is very good, confirming uniform strand properties and uniform transport current distribution during the cable test.

V. Conductor Qualification in Magnet Coils

The information obtained from model magnet tests is crucial to understanding the behaviour of the conductor and, especially, to optimize its specifications and properties for use in actual accelerator magnets. Thanks to the progress in Nb_3Sn accelerator magnet technology in the US and elsewhere, the available statistics of such magnet tests has increased, thereby offering insight into the interplay between conductor and magnet behaviour.

Table III shows in black the values of subelement sizes of RRP® wires that produced stable Nb_3Sn magnet performance down to 1.9 K and in the lightest gray those that did not lead to optimal performance. The subelements values in between are shown in the boxes in an intermediate shade of grey. The conclusions were made based on strand, cable and magnet test results. The stack number in the Table represents the number of total hexagonal superconducting bundles and Cu units in the strand layout. The subelement sizes for the various stack designs and strand diameters were provided by OST. From the Table the acceptable D_s for Nb_3Sn accelerator magnets is 40-45 µm or less. Such D_s range includes the combined effects of cable packing factor, J_c and *RRR* variations of cables used in magnet models.

TABLE III
Subelement Sizes in RRP Multi-Stack Strands

Stack design	Strand/sub-element size				
	0.5 mm	0.6 mm	0.7 mm	0.8 mm	1.0 mm
61	42 µm	51 µm	59 µm	68 µm	85 µm
91	34 µm	41 µm	48 µm	55 µm	69 µm
127	29 µm	35 µm	41 µm	47 µm	59 µm
169	26 µm	31 µm	36 µm	42 µm	52 µm
217	23 µm	27 µm	32 µm	36 µm	45 µm

In addition to producing stable magnet performance down to 1.9 K, wires with subelement values of ~40 µm produce coil re-magnetization at currents close to typical LHC injection currents, making for simpler corrections. Magnetic measurements of the Transfer Function and field harmonics of 11 T dipole models show that subelement values of ~40 µm are acceptable also for coil magnetization [12].

Whereas a large number of developing Nb_3Sn magnet models have been made with relatively small strand sizes (i.e. 0.7 mm) [10], [13]-[15], for the LHC luminosity upgrades a new IR quadrupole design with 150 mm aperture is foreseen based on larger cables made of 0.85 mm wire [3]. This is because in general, accelerator magnets are more efficient when using larger strands. Another example is the present dipole and quadrupoles conceptual designs for a muon collider Higgs factory, which are based on 1 mm strands [5]. For a serious prospect of Nb_3Sn use in actual accelerators magnets, it is therefore crucial to keep pushing strand development further, to produce acceptable wires with adequate number of stacks, in particular RRP 217 stack design, also for these larger wires.

VI. Conclusion

Conductor properties (strand and cable) determine key accelerator magnet parameters, including minimum and maximum operation fields, margin, and field quality. Conversely, the information obtained from magnet tests is crucial to understanding the behaviour of the conductor. A conductor qualification plan was proposed and implemented on a number of RRP conductors to evaluate possible candidates for the production magnets for the LHC upgrades. It was shown that 150 mm IR quadrupoles for the LHC luminosity upgrades when using 0.85 mm RRP strands will need strand design with 217 subelements to provide stable magnet operation at 1.9 K and low coil magnetization effects. It was also shown that under plastic deformation from either flat-rolling or Rutherford cabling, RRP wires with Ti doping retain larger values of critical current and of *RRR* than Ta-alloyed RRP wires.

Appendix

The commissioning of a variable-temperature probe designed [7] to perform strain sensitivity measurements in Helium on both LTS and HTS wires is herein described. The sample is wound and soldered onto a helical Walters' spring device, which is fixed at one end and subjected to a torque at the free end. Two concentric copper tubes act dually as 2000 A current and 60 Nm torque carriers. The torque is generated via a worm-gear setup and transmitted to the sample through the inner tube and spring assembly. Springs made either of Ti-6Al-4V or of CuBe were used. The setup was calibrated at room temperature, both in the horizontal and vertical positions, to also measure the effect of weight.

Fig. 1A shows the results for the circumferential strain for three different rotation angles as a function of the z location along the spring helix, as obtained with both the analytical (dashed line) and Finite Element models [7]. The latter predicts a sinusoidal behavior of the strain, with the amplitude increasing with increasing angular displacement. Three active strain gauges SG1, SG2 and SG3 and a dummy were mounted on a Ti-6Al-4V spring (Fig. 2A). The dummy was used as a

passive, temperature-sensing element. It was mounted transverse to the principal axis of strain and in close thermal contact with the spring, but not bonded to it. The strain gauge that was chosen is the Vishay WK-05-062AP-350, which is for use with Ti alloys. The active strain gauges were placed close to the center of the external magnet and 180 deg. apart in correspondence to the peaks and valleys of the expected sinusoidal strain distribution.

The instruments used in the DAQ were a SCXI-1520 (eight channel module for interfacing strain gauge Quarter, Half and Full-Bridges), a SCXI-1314 terminal block and a NI PCI 6289 DAQ Card. Each of SG1 and SG2 strain gauge was made part of a Quarter-Bridge type I circuit configuration, whereas SG3 was connected with the dummy in a Quarter-Bridge type II circuit configuration. Fig. 2A shows the SG1, SG2 and SG3 strain values measured at room temperature on the Ti-6Al-4V spring with the setup in vertical position as a function of positive (tensile) angular displacements. Fig. 3A (top) shows the measurements during the ramping of the angle from zero to 70 deg., and Fig. 3A (bottom) shows them during the ramping down from 70 deg. to zero. In both plots the experimental data are compared to the strain values from the analytical model. The strain gauges measurements were consistent with the Finite Element model predictions, with a 6-7% relative difference between the strain measured close to the sinusoid peaks by SG2 and SG3 and that measured close to a minimum by SG1 (Fig. 1A).

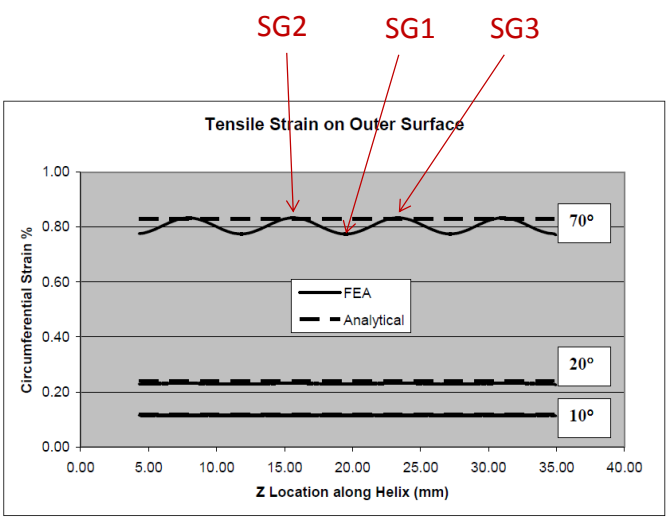

Fig. 1A. Circumferential strain for three different rotation angles as a function of the z location along the spring helix, as obtained with both the analytical (dashed line) and Finite Element models [23].

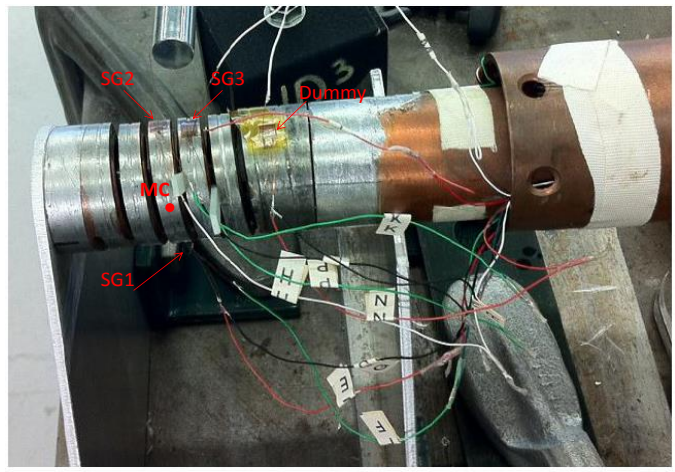

Fig. 2A. The active strain gauges were placed close to the center of the external magnet, and 180 deg. apart in correspondence to the peaks and valleys of the expected sinusoidal strain distribution.

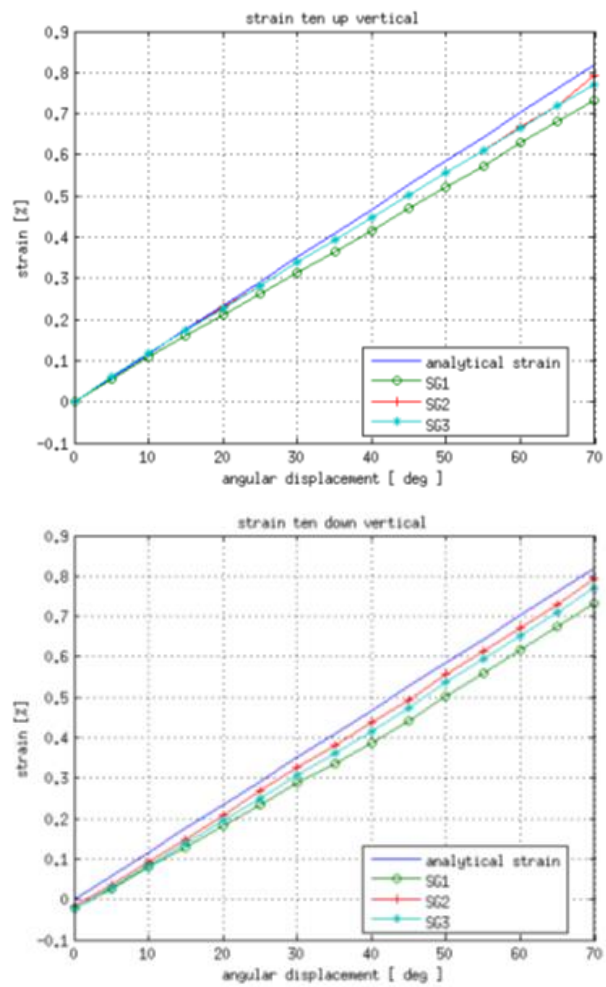

Fig. 3A. SG1, SG2 and SG3 strain values measured at room temperature on the Ti-6Al-4V spring with the setup in vertical position as a function of positive (tensile) angular displacements. Top plot shows the measurements during the ramping of the angle from zero to 70 deg., and bottom plot shows them during the ramping down from 70 deg. to zero. In both plots the experimental data are compared to the strain values from the analytical model.

After calibration, the setup was commissioned for critical current testing using Nb_3Sn RRP4 wires. RRP4 strand samples 1.83 m long were wound on grooved cylindrical barrels made

of stainless steel, and heat treated in Argon atmosphere. After reaction, the samples were transferred onto a CuBe Walters' spring and soldered on it along all of their length. A couple of sample end turns were used in the transition area from the Cu lugs to the spring. The critical current I_c was determined from the voltage-current (*V-I*) curve using a 0.1 μV/cm electrical field criterion. In order to determine what decrease in measured critical current to interpret as strain degradation, the precision of I_c and *n-value* measurements was measured by repeating the test at a fixed field and strain a number of times. The precision of the I_c was within 0.1 A and that of the *n-value* was within 0.2.

Four pairs of voltage taps were used. Three pairs were placed in series along the sample 10 cm apart, and one pair at the Cu leads to be used for quench protection. Such voltage taps are indicated as CH1, CH2, CH3, and CH4 in the schematic of Fig. 4A.

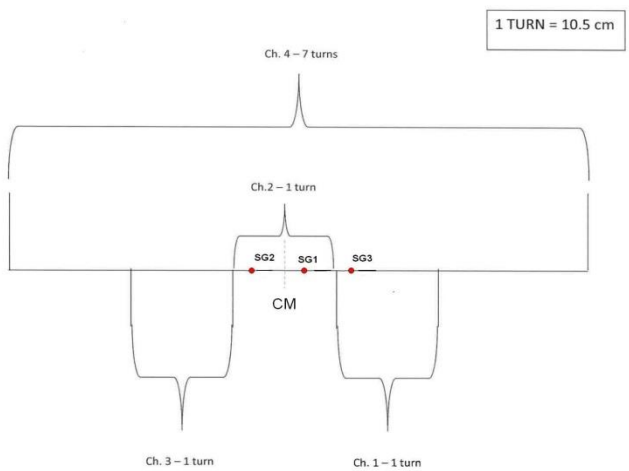

Fig. 4A. Schematic of voltage taps on Walters' spring shown relative to SG1, SG2 and SG3 strain locations.

Two identical samples of Ti-doped 132/169 RRP® (RRP4) wire were used for commissioning and to test reproducibility. Their heat treatment cycle was 72 h at 210ºC, 48 h at 400ºC and 50 h at 650ºC. Their I_c strain dependence was measured at 15 T and 4.2 K over channels CH1, CH2 and CH3. The best I_c reproducibility was obtained for CH1. Fig. 5A shows the I_c(15 T) as function of longitudinal strain over channel CH1 for both samples. The plot also shows the I_c(15 T) values obtained when performing standard I_c measurements on Ti-alloy ITER-type barrels. Such I_c values indicate that standard round samples see a compressive intrinsic strain of ~0.2 % at 4.2 K. Attempts at measuring the irreversible strain were also performed during the reproducibility studies. As point B in Fig. 5A shows, the first sample was tested up to +0.68% of absolute strain (+0.31% of intrinsic strain) before going back to point B' at zero intrinsic strain, where a noticeable I_c degradation was observed. The second sample was therefore tested up to point A at +0.63% of absolute strain (+0.26% of intrinsic strain). When going back to point A' at zero intrinsic strain, no I_c degradation was observed. An irreversible intrinsic strain range of +0.26% to +0.31% was therefore determined for these Ti-doped RRP4 wires.

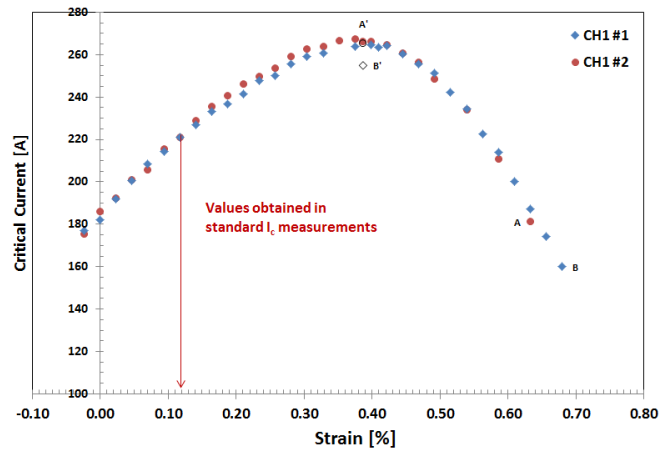

Fig. 5A. I_c(4.2 K, 15 T) as function of longitudinal strain over channel CH1 for both samples of 132/169 RRP® wire RRP4.

ACKNOWLEDGMENT

The authors are grateful to Allen Rusy for the assembly and alignment of the cabling machine's new turk-head and for operating and maintaining the machine, to Tom VanRaes for strain gauge mounting and Walters' spring and other sample preparation, to Marianne Bossert for strand and cable sample polishing and microscopy, to Ryuji Yamada for coordinating strand procurement, to Nandhini Dhanaraj for helping during the Walters' spring commissioning, and to Vito Lombardo for contributing to testing and analysis.

REFERENCES

[1] M. B. Field et al., "Internal tin Nb_3Sn conductors for particle accelerator and fusion applications", *Advances in Cryogenic Engineering*, vol. 54, AIP, V. 986, pp. 237–243 (2008).

[2] A. Kikuchi et al., "Cu Stabilized Nb_3Al Strands for the High Field Accelerator Magnet", IEEE Trans. Appl. Sup., V. 18, No. 2, p. 1026 (2008).

[3] E. Todesco et al., "Design Studies for the Low-Beta Quadrupoles for the LHC Luminosity Upgrade", accepted in IEEE Trans. Appl. Sup., V. 23, No. 3 (2013), p. 4002405.

[4] M. Karppinen et al., "Design of 11 T Twin-Aperture Nb_3Sn Dipole Demonstrator Magnet for LHC Upgrades", IEEE Trans. on Applied Superconductivity, Volume 22, Issue 3, June 2012 Page(s): 4901504

[5] A.V. Zlobin et al., "Preliminary Design of a Higgs Factory μ+μ- Storage Ring", Proc. of IPAC2013, Shanghai, China, May 2013, p. 1487.

[6] E. Barzi et al., "Superconducting strand and cable development for the LHC upgrades and beyond", accepted in IEEE Trans. Appl. Sup., V. 23, No. 3 (2013).

[7] E. Barzi et al., "Design of a Probe for Strain Sensitivity Studies of Critical Current Densities in Superconducting Wires", IEEE Trans. Appl. Sup., V. 20, No. 3, p. 1626 (2010).

[8] E. Barzi et al., "Commissioning of 14T/16T Rutherford Cable Test Facility with Bifilar Sample and Superconducting Transformer", submitted to CEC/ICMC 2013 for publication in AIP.

[9] E. Barzi et al., "Studies of Nb_3Sn Strands based on the Restacked-Rod Process for High-field Accelerator Magnets", *IEEE Trans. Appl. Sup.*, V. 22, No. 3, pp. 6001405 (2012).

[10] A.V. Zlobin et al., "Development of Nb_3Sn 11 T single aperture demonstrator Dipole for LHC Upgrades", Proc. of the 24th Particle Accelerator Conference (PAC 2011), pp. 1460-1462, March 28 - April 1, 2011, New York, USA.

[11] E. Barzi et al., "Development and Fabrication of Nb_3Sn Rutherford Cable for the 11 T DS Dipole Demonstration Model", IEEE Trans. Appl. Sup., V. 22, No. 3, pp. 6000805 (2012).

[12] N. Andreev et al., "Field quality measurements in a single-aperture 11T Nb_3Sn demonstrator dipole for LHC upgrades", IEEE Trans. on Appl. Supercond., Vol. 23, Issue 3, June 2013 Page 4001804.

[13] S. Caspi et al., "Fabrication and Test of TQS01 – a 90mm Nb3Sn Quadrupole Magnet for LARP", IEEE Trans. on Applied Superconductivity, Volume 17, Issue 2, June 2007 Page(s):1122-1125.
[14] S. Feher et al., "Development and Test of LARP technological quadrupole (TQC) magnet", IEEE Trans. on Applied Superconductivity, Volume 17, Issue 2, June 2007 Page(s):1126-1129.
[15] G. Ambrosio et al., "LARP Long Nb_3Sn Quadrupole Design", IEEE Trans. on Appl. Supercond., Vol. 18, Issue 2, June 2008 p. 268.